

# BAYESIAN MASS AVERAGING

Pranay Seshadri\*, Andrew Duncan, George Thorne

Imperial College London, London, U. K.  
Rolls-Royce plc., Derby, U. K.

## Abstract

Mass averaging is pivotal in turbomachinery. In both experiments and CFD simulations mass averages of flow quantities may be taken circumferentially, radially, and often both. These are critical for arriving at 1D or 2D performance metrics that shape our understanding of losses and their control. Such understanding empowers design advances, affords anomaly detection, informs maintenance and diagnostic efforts. This paper presents a new statistical framework for obtaining mass averages of flow quantities in turbomachinery, tailored for rig tests, heavily instrumented engines, and cruise-level engines. The proposed Bayesian framework is tailored for computing mass averages of pressures and temperatures, given their values from circumferentially scattered rakes. Two variants of this methodology are offered: (i) for the case where massflow rate distributions can not be experimentally determined and computational fluid dynamics (CFD) based profiles are available, and (ii) where experimental massflow rate distributions are available. In scope, this framework addresses limitations with existing measurement budget calculation practices and with a view towards facilitating principled aggregation of uncertainties over measurement chains.

## 1 Introduction

Flow averaging underpins aerothermal insight. In their seminal paper, Cumpsty and

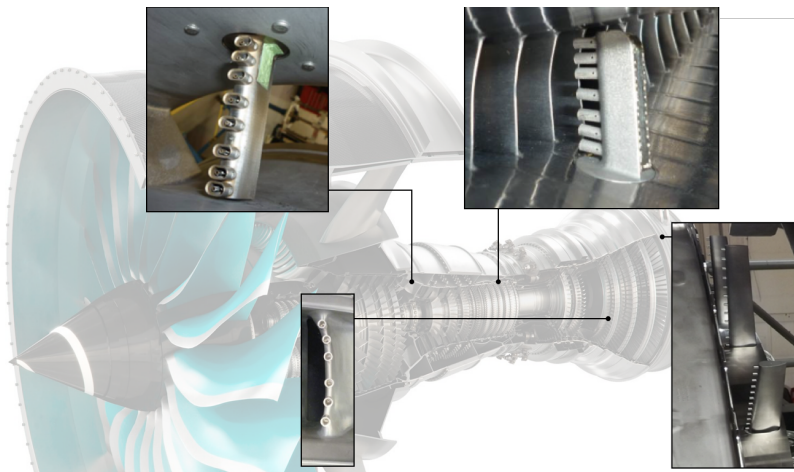


Figure 1: Different rakes and their locations in an engine.

Horlock [1] detail the importance of mass averaging for both pressure and temperature

---

\*Address all correspondence to [p.seshadri@imperial.ac.uk](mailto:p.seshadri@imperial.ac.uk)

measurements. The ability to accurately estimate the average temperature, pressure and velocity at any axial location within the gas path can catapult advances in aerothermal technology. This would undoubtedly deliver safer, less noisy, more efficient and cleaner sub-systems in aeroengines, having an immeasurable impact on the way humanity flies. Today, the closest representation of the flow-field stems from a range of computational fluid dynamics (CFD) hierarchies where greater accuracy is often traded-off with complexity in geometry and flow-feature resolution. The challenge with CFD as a tool is that it is wedded to the boundary conditions and geometries supplied. It cannot capture what we do not know of the engine environment and the uncertainties therein. In contrast, sensor-based measurements gathered from test-bed data—i.e., in-flight tests, on-ground engine tests and rigs—offer a more accurate representation of flow through an engine. However, they lack the spatial resolution required, making flow-field extrapolation and computation of averages a challenge.

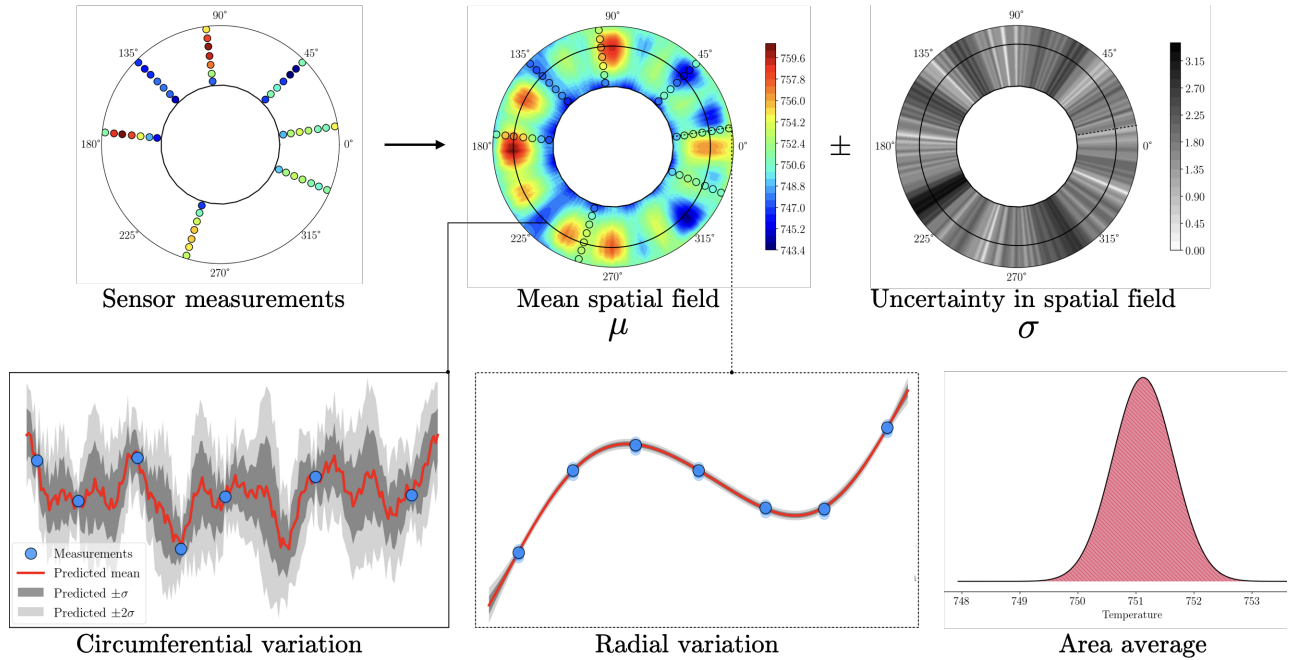


Figure 2: The Bayesian aerothermal model presented in [2] that uses sensor measurements and assumptions on the spatial harmonics to arrive at an area average probability distribution.

Today’s aeroengine measurements are undertaken using a myriad of sensors, ranging from K- and N-type thermocouples and platinum resistance thermometers (PRT) for temperature measurements, to a variety of transducers for pressure measurements (see Figure 1). Depending on the local environment surrounding each rake, sensors are carefully selected to offer precise and consistent measurements over time with minimal drift. The housing and shielding of these sensors is also an important design consideration, as the sensors need to be exposed to the correct flow conditions whilst having minimal impact on the flow itself. There is an ever-increasing body of open literature devoted to the study of sensor shrouds (see [3, 4]).

Concurrently, there has been interest in the problem of spatial flow-field estimation and

its subsequent area averaging with the current authors proposing both frequentist [5, 6] and Bayesian approaches [2]. The latter is particularly advantageous as it offers a principled approach using the rich framework of Gaussian processes for accounting for both error in the measurements and uncertainty in the model. Consider the schematic in Figure 2 that comprises sensor measurements from a series of radially positioned probes on several circumferentially placed rakes. The Bayesian workflow in [2] is used to infer the predicted spatial pattern and its uncertainty using a Gaussian process model with a bespoke physics-inspired covariance kernel. This kernel in turn is parameterized by a set of hyperparameters that tune the extent of correlation between the different sensor values. In a Bayesian context, they can be ascertained by imposing priors on the hyperparameters that are updated based on the data using Markov chain Monte Carlo (MCMC). The resulting statistical framework is powerful for extracting inference—from accounting for model mis-specification and noisy data, to offering recipes for optimal sensor placement and estimates of uncertainty [2]. Perhaps of greatest value is the notion that this approach can yield an area average probability density function, as shown in Figure 2. This single graph captures the model and measurement uncertainty in a rigorous manner.

That said, one limitation of a probabilistic description of the area average is that existing area-to-mass conversion factors can not be adapted or used. At most measurement planes, the mass flow distribution will be greatest at mid-span and diminished towards the endwalls. Consequently, the spatial mean, and more importantly, the spatial variance towards the hub and the casing will have a smaller contribution to the mass average, compared to the spatial mean and variance elsewhere. Thus, a conversion from the area to mass average cannot be solely expressed via a multiplicative factor of the area average mean and variance. Rather than carry out operations on the area average probability distribution itself, it makes more sense to multiply the spatial temperature (or pressure) field by an assumed (or known) mass flow rate distribution, and then compute the mass weighted integral spatially. It is precisely this idea that is pursued in this paper; we present two strategies for attaining a mass average distribution using Bayesian inference.

The remainder of this paper is structured as follows. A cursory summary of the key principles behind Bayesian inference is presented in 2. This sets the stage for the proposed mass averaging formulations that are introduced in 3, which is followed by numerical examples in 4.

## 2 Bayesian inference

This section presents a brief overview of the key ideas underpinning Bayesian inference. For further details, interested readers are encouraged to consult [7, 8].

### 2.1 Bayes’ rule, prediction and likelihood

Let us assume the existence of a model that yields the spatial distribution of temperature or pressure (as in Figure 1). Further, let  $\alpha$  denote an unobservable vector-valued input to this model, giving  $\alpha$  the interpretation as its model parameters. Given the rather limited information afforded to us, it seems rational to assign  $\alpha$  a probability distribution  $\mathbb{P}(\alpha)$  rather than a fixed value. This is called the prior.

The observations from the few circumferentially- and radially-placed sensors are denoted

by the vector  $y$ , where  $y = (y_1, \dots, y_n)$  for each of the  $n$  sensors. To draw inference regarding  $\alpha$  given  $y$ , one requires a model of the *joint probability distribution*  $\mathbb{P}(\alpha, y)$ , which may be expressed as

$$\mathbb{P}(\alpha, y) = \mathbb{P}(\alpha) \mathbb{P}(y|\alpha) = \mathbb{P}(y) \mathbb{P}(\alpha|y) \quad (1)$$

where the term  $\mathbb{P}(y|\alpha)$  is called the *data distribution*. When interpreting this distribution for a fixed  $y$  strictly as a function of  $\alpha$ , one refers to  $\mathbb{P}(y|\alpha)$  as the *likelihood function* [7]. In Bayesian inference, we are interested in ascertaining the conditional probability of the model parameters  $\alpha$  given observations  $y$

$$\mathbb{P}(\alpha|y) = \frac{\mathbb{P}(\alpha) \mathbb{P}(y|\alpha)}{\mathbb{P}(y)}, \quad (2)$$

which is known as Bayes' rule and  $\mathbb{P}(\alpha|y)$  is termed the *posterior density*. Succinctly stated, the objective of Bayesian inference is to develop  $\mathbb{P}(\alpha, y)$  and undergo calculations to determine  $\mathbb{P}(\alpha|y)$  (see pages 6-7 of [7]). Note that the denominator in (2) can also be expressed as an integral (also termed marginalization)

$$\begin{aligned} \mathbb{P}(y) &= \int \mathbb{P}(y|\alpha) \mathbb{P}(\alpha) d\alpha \\ &\propto \mathbb{P}(y|\alpha) \mathbb{P}(\alpha). \end{aligned} \quad (3)$$

where we refer to  $\mathbb{P}(y)$  as the one of the *marginal distributions* of the joint distribution  $\mathbb{P}(\alpha, y)$ .

## 2.2 Gaussian process regression

Gaussian processes represent a powerful and flexible class of models for predicting spatially- and temporally-varying scalar- and vector-valued functions, where any finite-dimensional marginal distribution of the covariates is a Gaussian distribution [7]. A Gaussian process  $f$  for a quantity of interest  $\mathcal{Q}$  can be defined in terms of its mean  $\mu_{\mathcal{Q}}$  and covariance function  $\Sigma_{\mathcal{Q}}$  [9], i.e.,

$$f(x) \sim \mathcal{N}(\mu_{\mathcal{Q}}(x), \Sigma_{\mathcal{Q}}(x, x)). \quad (4)$$

If we represent our *training data* as  $\mathcal{D} := \{x_i, y_i\}_{i=1}^n$  and *testing data* locations as  $x^* = (x_1^*, \dots, x_m^*)$ , then the mean and covariance functions of the Gaussian process is given by

$$\begin{aligned} \mu_{\mathcal{Q}}(x^*) &= K(x^*, x) (K(x, x) + \Sigma)^{-1} y \\ \Sigma_{\mathcal{Q}}(x^*, x^*) &= K(x^*, x^*) - K(x^*, x) (K(x, x) + \Sigma)^{-1} K(x, x^*). \end{aligned} \quad (5)$$

Here  $\Sigma = \sigma^2 \mathbf{I}$  is a diagonal matrix of the measurement noise associated with each sensor. We assume a Gaussian noise model, i.e., our observations  $y$  are corrupted by a zero-mean noise  $\mathcal{N}(0, \sigma^2)$ . The matrix  $K(\cdot, \cdot)$  in (5) represents the *kernel function*  $k$  evaluated at the input arguments. This function represents the covariance between any two points and controls the smoothness of samples from the Gaussian process along with the extent of shrinkage towards the mean [7]. Kernel functions are typically parameterized by *hyperparameters* that need to be tuned based on the data.

The kernel functions used in this paper are based on those in [2], and include a Fourier series kernel in the circumferential direction and a squared exponential kernel in the radial

direction. We omit these expressions here and refer the reader to Section 2 of that text. There are two *hyperparameters* for the squared exponential component, i.e., a correlation length  $l$  and a kernel noise  $\sigma_f$ , that are assigned the following prior distributions

$$l \sim \mathcal{N}^+(0, 1), \quad \text{and} \quad \sigma_f \sim \mathcal{N}^+(0, 1), \quad (6)$$

where the symbol  $\mathcal{N}^+(0, 1)$  indicates a half normal distribution with a mean of zero and a variance of unity. In the circumferential direction, provided one can prescribe the frequencies of the circumferential harmonics, priors can be assigned to both the sine and cosine components of each frequency. Following Seshadri et al., we set these priors

$$\lambda_j \sim \mathcal{N}^+(0, 1), \quad \text{for } j = 1, \dots, 2w + 1 \quad (7)$$

where  $w$  represents the number of harmonics. The last prior we assign is for the noise  $\sigma$ , which we assume lies between zero and an upper bound  $\epsilon$  that is dependent on the measurement chain and sensor measurement precision,  $\mathbb{P}(\sigma) = \mathcal{U}[0, \epsilon]$ . For ease in notation, we group all our priors (apart from the noise) into  $\mathbb{P}(\chi)$ , where  $\chi = (l, \sigma_f, \lambda_1, \dots, \lambda_{2k+1})$ , and thus with a slight abuse in notation we write  $\mathbb{P}(\chi) = \mathcal{N}^+(0, 1)$ , which is a  $(2k + 3)$ -dimensional distribution. This sets the stage for a computational approach for estimating the posterior distributions of our hyperparameters.

### 2.3 Bayesian inference in Gaussian process regression

As Gaussian process regression is a strictly non-parametric framework, the model parameters  $\alpha$  in (2) cannot be directly substituted by  $\chi$ . In the Gaussian process model given by  $f$  in (4), the likelihood function is given by  $\mathbb{P}(y|f, \sigma) = \mathcal{N}(f, \sigma^2 I)$  and the prior at the observed inputs is  $\mathbb{P}(f|x, \chi) = \mathcal{N}(0, K)$ . The conditional evidence of the Gaussian process can then be computed via

$$\mathbb{P}(\mathcal{D}|\sigma, \chi) := \mathbb{P}(y|x, \sigma, \chi) = \int \mathbb{P}(y|f, \sigma) \mathbb{P}(f|x, \chi) \mathbb{P}(\chi) \mathbb{P}(\sigma) df d\sigma d\chi. \quad (8)$$

The expression on the left hand side is the probability of observing the data, conditioned upon the hyperparameter values  $\sigma, \chi$ , and the kernel encoded in  $\mathbb{P}(f|x, \chi)$ . The standard approach for integrating (8) is to use Markov chain Monte Carlo (MCMC), from which posterior probability densities of the hyperparameters can be obtained. The challenge with MCMC however is that it may necessitate long running times, particularly as the number of frequencies increase—increasing the number of hyperparameters that need to be tuned. One workaround is to focus on the probability density associated with (8) and ignore its probability mass. More specifically, we solve a gradient-based optimisation problem for identifying the mode of  $\mathbb{P}(\mathcal{D}|\sigma, \chi)$  rather than its full distribution [10]. This is known as the *maximum a posteriori* (MAP) estimate and is given by

$$\underset{\sigma, \chi}{\text{maximize}} \quad \mathbb{P}(y|f, \sigma) \mathbb{P}(f|x, \chi) \mathbb{P}(\chi) \mathbb{P}(\sigma). \quad (9)$$

This optimisation problem is generally non-convex, but automatic differentiation methods can be used to extract gradients that can help guide the optimizer. Further particulars on the assumptions underpinned by MAP and its similarity to maximum likelihood estimation can be found in [9]. Our adoption of MAP in this paper, instead of MCMC, is motivated the need to compute real-time mass average estimates during engine tests. That said, for post-test aerothermal insight, MCMC should be used.

### 3 Bayesian mass average

Let  $\mathcal{Q}(r, \theta)$  denote the spatial variation of temperature or pressure. Our goal is to compute the mass average of this quantity

$$\bar{\mathcal{Q}}_{\dot{m}} = \frac{\int_0^{2\pi} \int_{r_i}^{r_o} \mathcal{Q}(r, \theta) \dot{m}(r, \theta) r dr d\theta}{\int_0^{2\pi} \int_{r_i}^{r_o} \dot{m}(r, \theta) r dr d\theta}, \quad (10)$$

where  $\dot{m}(r, \theta)$  is the massflow rate distribution. For simplicity, we assume that our integration bounds in the radial direction vary from  $[0, 1]$  instead of  $[r_i, r_o]$ . This results in the following substitution

$$\bar{\mathcal{Q}}_{\dot{m}} = \frac{(r_o - r_i) \int_0^{2\pi} \int_0^1 \mathcal{Q}(r, \theta) \dot{m}(r, \theta) h(r) dr d\theta}{(r_o - r_i) \int_0^{2\pi} \int_0^1 \dot{m}(r, \theta) h(r) dr d\theta} \quad (11)$$

where  $h(r) = r(r_o - r_i) + r_i$ . The goal of this section is to analytically compute  $\bar{\mathcal{Q}}_{\dot{m}}$  when  $\mathcal{Q}(r, \theta)$  is a Gaussian process.

#### 3.1 Polynomial massflow rate distribution

To simplify matters, we adopt the rationale that the massflow rate distribution is uniform in the circumferential direction, leading to

$$\bar{\mathcal{Q}}_{\dot{m}} = \frac{\int_0^{2\pi} \int_0^1 \mathcal{Q}(r, \theta) \dot{m}(r) h(r) dr d\theta}{\int_0^{2\pi} \int_0^1 \dot{m}(r) h(r) dr d\theta}. \quad (12)$$

Note that the numerator within the integral in (12) can be interpreted as a random Gaussian field multiplied by a constant, which is also a Gaussian process. This quantity is then integrated—a specific linear operator acting on a Gaussian process—resulting in another Gaussian process, given by

$$\begin{bmatrix} y \\ \psi \int y^*(z) \dot{m}(z) h(r) dz \end{bmatrix} \sim \mathcal{N} \left( \begin{bmatrix} 0 \\ 0 \end{bmatrix}, \begin{bmatrix} K(x, x) + \Sigma & \psi \int K(x, z) \dot{m}(z) h(r) dz \\ \psi \int K(x, z) \dot{m}(z) h(r) dz & \psi^2 \int \int K(z, z) \dot{m}^2(z) h^2(r) dz dz \end{bmatrix} \right), \quad (13)$$

where for notational brevity we set  $z$  is a proxy for  $x = (r, \theta)$  and

$$\psi = \frac{1}{\int_0^{2\pi} \int_0^1 \dot{m}(r) h(r) dr d\theta}, \quad (14)$$

and the definitions of the kernel  $K$  hold from before. Symbolic integration packages such as **Mathematica** and **Matlab** can be used to analytically evaluate the closed form expressions above from which the mean and variance in the mass averaged quantity  $\mathcal{Q}$  are given as

$$\mu_{\bar{\mathcal{Q}}_{\dot{m}}} = \psi \int K(x, z) \dot{m}(r) h(r) dz \cdot (K(x, x) + \Sigma)^{-1} y \quad (15)$$

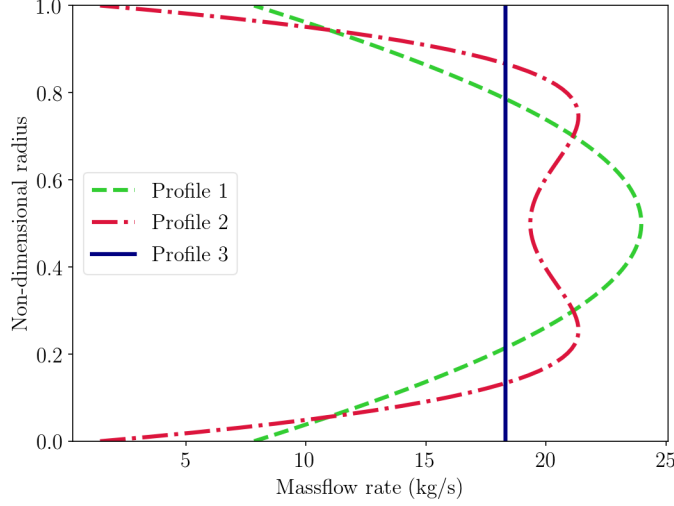


Figure 3: Three sample massflow rate profiles.

and

$$\sigma_{\mathcal{Q}_{\dot{m}}}^2 = \psi^2 \int \int K(z, z) \dot{m}^2(r) h^2(r) dz dz - \psi \int K(x, z) \dot{m}(r) h(r) dz \cdot (K(x, x) + \Sigma)^{-1} \psi \int K(x, z) \dot{m}(r) h(r) dz. \quad (16)$$

We assume that  $\dot{m}$  is (at least) a cubic polynomial that captures the variation in the massflow rate distribution. If a massflow rate distribution can be extracted from a representative CFD simulation, then the coefficients  $\{c_0, c_1, \dots, c_N\}$  corresponding to the polynomial fit

$$\dot{m}(r) = c_0 + c_1 r + c_2 r^2 + c_3 r^3 + \dots + c_N r^N \quad (17)$$

can be computed using a standard least squares with a Vandermonde matrix. Figure 3 shows a few different sample massflow rate distributions—each integrate to yield the same massflow rate area, i.e., they all have the area under the curve.

It should be noted that one can just as easily derive the integrals in (15) and (16) using other parametric curves, such as splines

$$\dot{m}(r) = c_0 + c_1 r + c_2 r^2 + c_3 r^3 + \sum_{i=1}^K \max[0, (r - s_i)], \quad (18)$$

where  $s_i$  corresponds to the spline knots. This does, however, increase the complexity of the expressions that must be integrated.

### 3.2 Gaussian random field for massflow rate

The random field for temperature (or pressure) can be written as  $\mathcal{N}(\mu_{\mathcal{Q}}, \Sigma_{\mathcal{Q}})$ . Using the same kernel functions in [2], or alternate ones, a random field for a massflow rate  $\mathcal{N}(\mu_{\dot{m}}, \Sigma_{\dot{m}})$  can also be obtained. As the product of two Gaussian distributions does not yield a Gaussian distribution, there is no closed form analytical solution that one can leverage for the mass



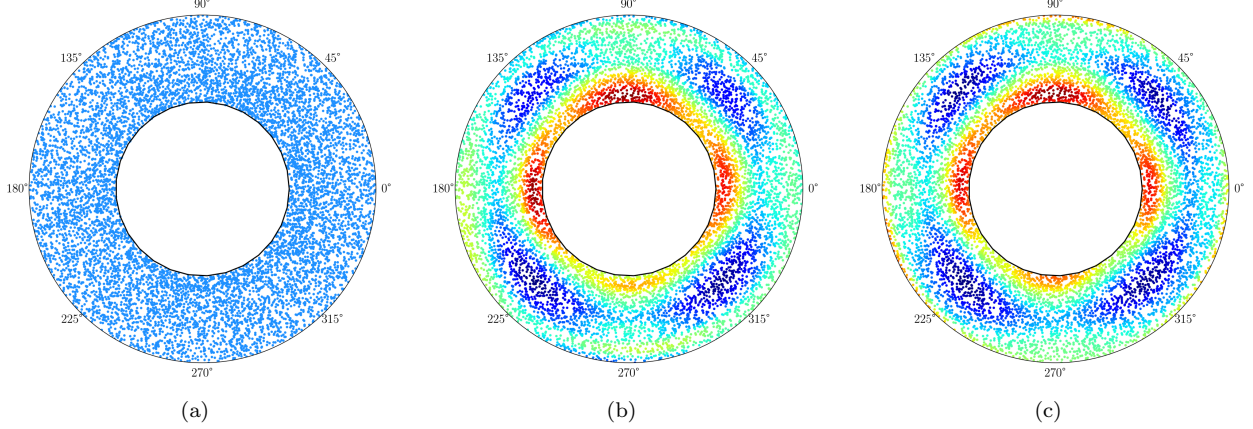


Figure 4:  $P$  spatially distributed points in (a) and two samples of temperature (b)  $t_1$  and (c)  $t_2$ , from  $\mathcal{N}(\mu_Q, \Sigma_Q)$  at the points in (a).

average when using a Gaussian random field for the massflow rate. Thus a discretized approach must be adopted.

Let  $\{(\tilde{\theta}_1, \tilde{r}_1), \dots, (\tilde{\theta}_P, \tilde{r}_P)\}$  be  $P$  randomly sampled coordinate locations; Figure 4(a) shows a sample when  $P = 10,000$ . Next, let  $t_1, \dots, t_L$  be  $L$  independent and identically distributed (iid) random samples from the distribution  $\mathcal{N}(\mu_Q, \Sigma_Q)$ . Each sample  $t_i$  is a vector of length  $P$ , corresponding to the  $P$  spatially randomly distributed coordinates. Let  $s_1, \dots, s_L$  also be  $L$  iid random samples from the distribution  $\mathcal{N}(\mu_{\dot{m}}, \Sigma_{\dot{m}})$ , where  $s_i$  is a vector of length  $P$  and is the massflow rate distribution evaluated at the same coordinates corresponding to  $t_i$ . The mass average of each sample is given by

$$\tilde{Q}_{\dot{m},i} = \frac{t_i^T \text{diag}(\tilde{r}) s_i}{s_i^T \tilde{r}}, \quad (19)$$

where  $i = 1, \dots, L$ ,  $\tilde{r} = (\tilde{r}_1, \dots, \tilde{r}_P)$  and  $\text{diag}(\cdot)$  is a diagonal matrix of the vector-valued argument. These mass average samples can be used to arrive at a histogram quantifying the mass average distribution; we demonstrate this in the following section in this text.

It is important to note that we have not bounded the massflow rate values, i.e., they can take on both positive and negative values. The latter may be misleading particularly when the mean massflow rates are low, but their standard deviations are large, implying that there may be realizations of the Gaussian process random field where there is reverse flow, when in reality that is simply a numerical modeling artifact. One way to tackle this is to construct the Gaussian process random field for  $\exp(\dot{m})$  instead of  $\dot{m}$ . Other approaches include the introduction of certain *ghost data points*, and the use of constraints on the hyperparameters to ensure that the standard deviations are realistic.

## 4 Numerical examples

The two aforementioned proposals for prescribing a mass flow rate distribution for arriving at a Bayesian mass average are illustrated below. Both proposals are demonstrated on temperatures from an isolated compressor measurement plane, taken from an on-ground



engine test. The rakes in this extract were placed at the same in-passage pitchwise location to avoid capturing the higher frequency blade-to-blade modes, i.e., although the rakes had different circumferential angles, their location relative to the upstream stators were fixed. The consequence of this placement, as mentioned in [5], is that the probes only see temperature variations associated with engine modes, i.e., leakage flows, upstream struts, casing ovalisation and other geometrical asymmetries. Provided the contribution of the blade-to-blade modes to the mean term of the Fourier expansion are negligible, then accurate area averages can be determined using only information afforded from the engine modes.

The codes used to generate the results in this paper were developed in `python` and use the open-source `pymc3` package [11] for Bayesian statistical modeling. Figure 5(a) and (b) plot the spatial mean and standard deviation in the temperature for this extract assuming frequencies 1, 2 and 4 are present in the pattern—using the priors mentioned in Section 2.2. A radial slice, taken at 0.94 radians is also captured in Figure 5(c). It is important to note how the kernels are able to appropriately capture the uncertainty at the endwalls and the uncertainty between measurements points.

#### 4.1 Polynomial massflow rate

The three different massflow rate profiles shown in Figure 3 are applied to the Gaussian random field mentioned above. Profile 1 has a parabolic trajectory, with a peak massflow rate of 24 kg/sec at mid-span. Profile 2 has a massflow rate distribution that is more representative of real engine conditions with a particular emphasis at the endwalls where the massflow rate decreases all the way to zero. Finally, Profile 3 is representative of a uniform massflow rate distribution in the radial direction. All three massflow rate profiles are assumed to be uniform in the circumferential direction. Thus, the expectation is that Profile 3 will yield the same mean and variance as the area average, while the other two will likely differ. One particular notion of interest is the difference in the mass average variance relative to the area average variance.

The results for the three profiles are shown in Figure 6 along with the Bayesian area average. As expected the mean and the variance for the area average are equivalent to that of Profile 3. It is interesting to note that Profiles 1 and 2 lead to distinctly different behaviors—in the former the variance is very slightly reduced compared to the area average, but there is about a 1K difference in the mean. Profile 2, which is more representative of a engine massflow rate distribution, has a very similar mean to the area average, but has a significant reduction in the variance.

#### 4.2 Gaussian random field for massflow rate

Using the same computational workflow as in Figure 2 (and Figure 5), a Gaussian random field model is generated for two hypothetical velocity rakes (density is assumed constant along the measurement plane) positioned at  $85^\circ$  and  $275^\circ$ , as shown in Figure 7. In the radial direction, the pattern follows a similar trend to Profile 2, while in the circumferential direction two spatial harmonics are present, corresponding to harmonics 1 and 12.

The mass average histogram obtained through the discretization procedure outlined in Section 4.2 is shown in Figure 8. It should be noted that although seemingly similar, this distribution is not Gaussian. As mentioned before, the product of two Gaussian random fields does not yield another Gaussian random field, motivating the discretized technique pursued

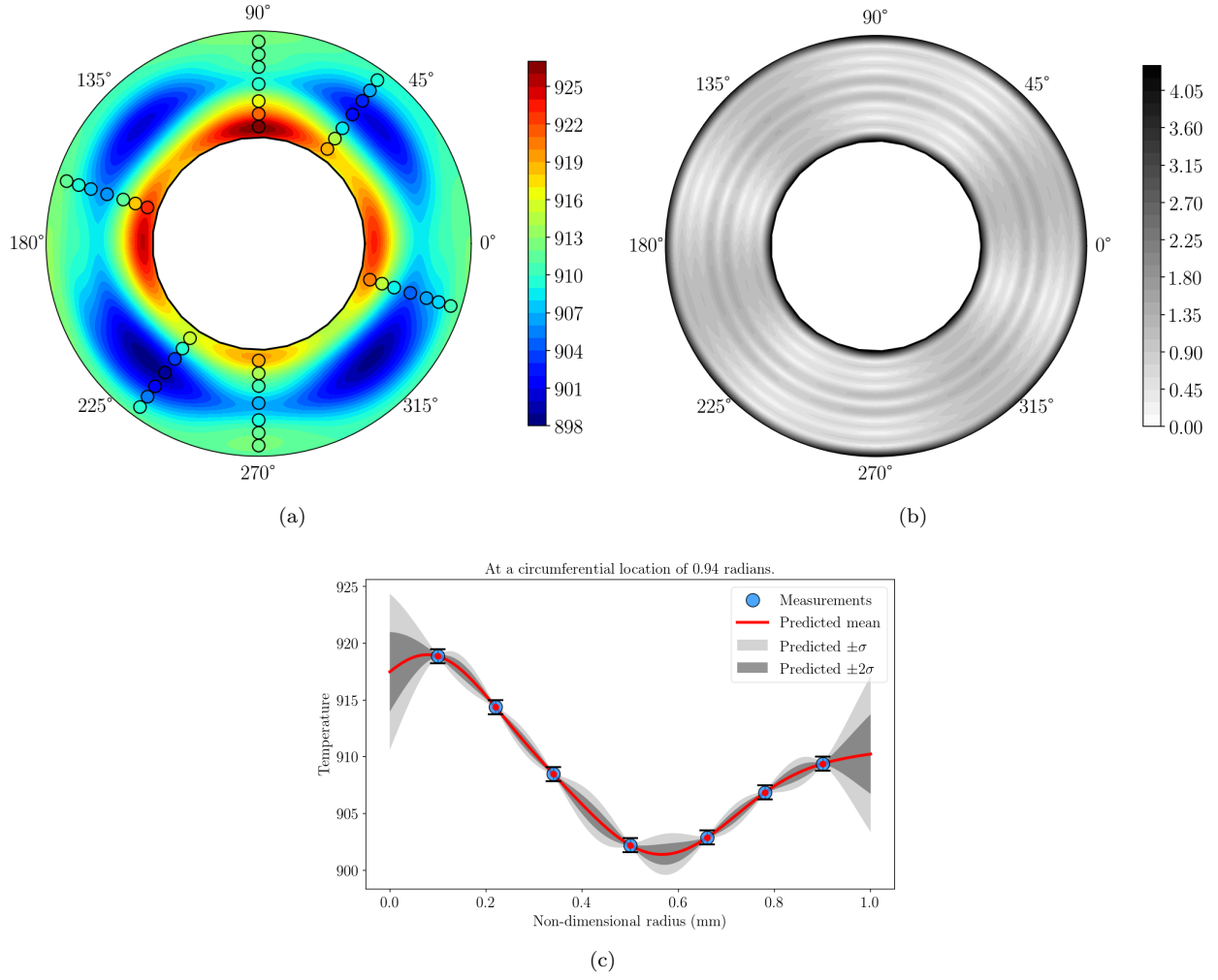


Figure 5: Gaussian process random field distributions for temperature: (a) annular spatial mean; (b) annular spatial standard deviation; (c) Radial slice at a circumferential location of 0.94 radians.

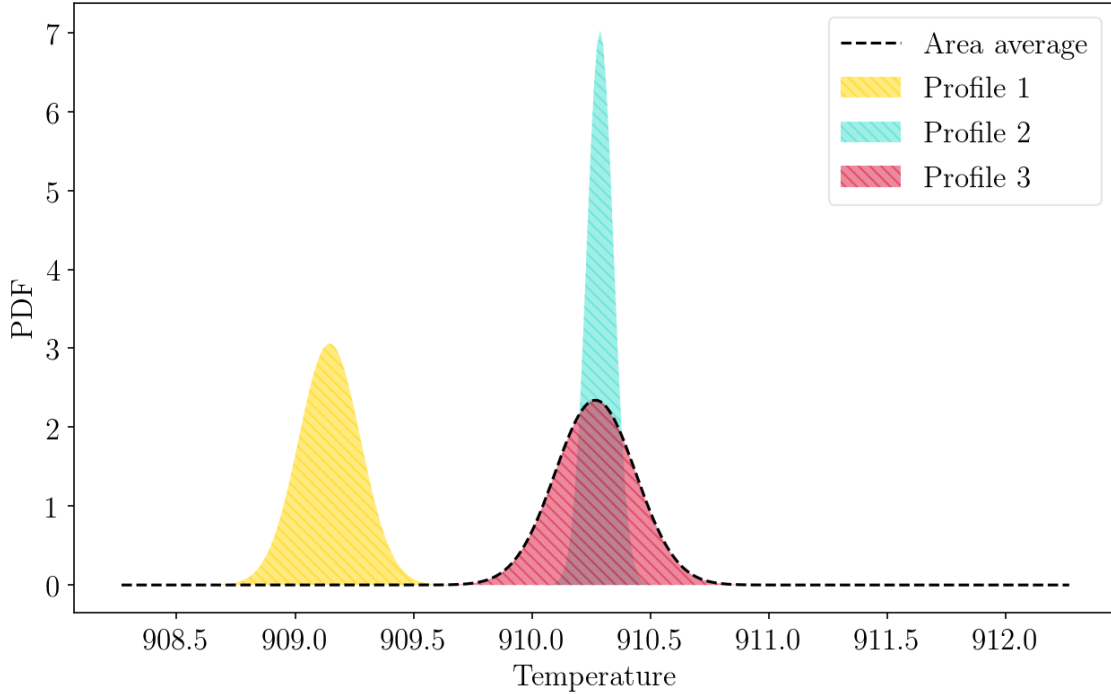


Figure 6: Comparison of the area and mass average probability density functions.

in this paper. To the best of the authors knowledge, this represents the most principled way to extract a mass average given measurements of either temperature or pressure and massflow.

## 5 Conclusions

In this paper, two new methods for more rigorous calculations of the mass average are proposed. These techniques leverage recent work on Bayesian methods for spatial flow-field approximation from real engine measurements. Over the upcoming few years, it is expected that these probabilistic methods will replace conventional averaging methods, that fall short of offering rigorous performance estimates.

## Acknowledgments

The authors are grateful to Raúl Vázquez Díaz (Rolls-Royce). This work was funded by Rolls-Royce plc; the authors are grateful to Rolls-Royce for permission to publish this paper.

## References

- [1] Cumpsty, N. A., and Horlock, J. H., 2006. “Averaging nonuniform flow for a purpose”. *Journal of turbomachinery*, **128**(1), pp. 120–129.

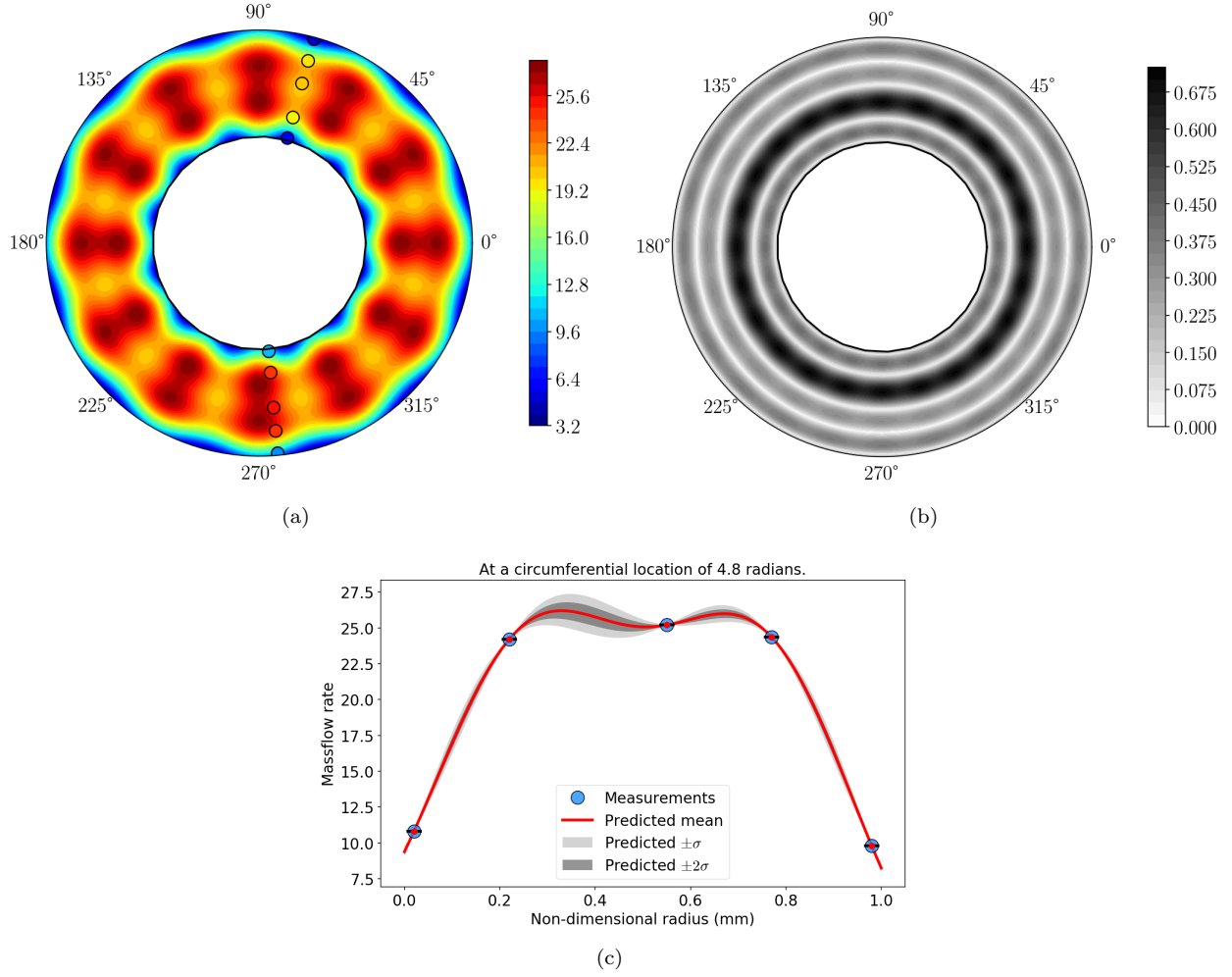


Figure 7: Massflow rate Gaussian process random field distributions for temperature: (a) annular spatial mean; (b) annular spatial standard deviation; (c) Radial slice at a circumferential location of 4.8 radians.

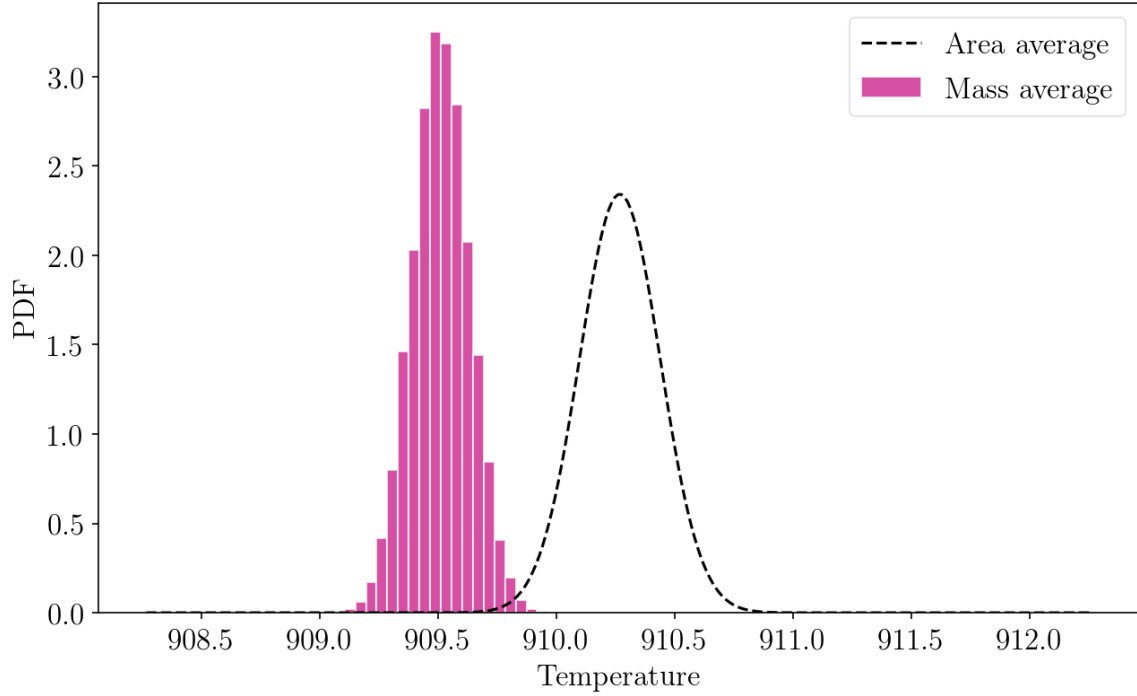


Figure 8: Comparison of the area and mass average probability density functions.

- [2] Seshadri, P., Duncan, A., Thorne, G., Parks, G., and Girolami, M., 2020. “Bayesian assessments of aeroengine performance”. *Forthcoming*.
- [3] Scillitoe, A. D., Ubald, B., Seshadri, P., and Shahpar, S., 2020. “Design Space Exploration Of Stagnation Temperature Probes Via Dimension Reduction”. In *Proc. ASME Turbo Expo*.
- [4] Bonham, C., Thorpe, S. J., Erlund, M. N., and Stevenson, R., 2017. “Combination probes for stagnation pressure and temperature measurements in gas turbine engines”. *Measurement Science and Technology*, **29**(1), p. 015002.
- [5] Seshadri, P., Simpson, D., Thorne, G., Duncan, A., and Parks, G., 2020. “Spatial flow-field approximation using few thermodynamic measurements—part i: Formulation and area averaging”. *Journal of Turbomachinery*, **142**(2).
- [6] Seshadri, P., Duncan, A., Simpson, D., Thorne, G., and Parks, G., 2020. “Spatial flow-field approximation using few thermodynamic measurements—part ii: Uncertainty assessments”. *Journal of Turbomachinery*, **142**(2).
- [7] Gelman, A., Carlin, J. B., Stern, H. S., Dunson, D. B., Vehtari, A., and Rubin, D. B., 2013. *Bayesian data analysis*. CRC press.
- [8] Kruschke, J., 2014. *Doing Bayesian data analysis: A tutorial with R, JAGS, and Stan*. Academic Press.
- [9] Rasmussen, C. E., and Williams, C. K., 2006. *Gaussian Processes for Machine Learning*. MIT Press.

- [10] Kuss, M., 2006. “Gaussian process models for robust regression, classification, and reinforcement learning”. PhD thesis, Technische Universität Darmstadt Darmstadt, Germany.
- [11] Salvatier, J., Wiecki, T. V., and Fonnesbeck, C., 2016. “Probabilistic programming in python using pymc3”. *PeerJ Computer Science*, **2**, p. e55.